Electrochemical Performance of Symmetric Solid-State Supercapacitors Based on Carbon Xerogel Electrodes and Solid-Polymer Electrolytes

Boryana Karamanova , Emiliya Mladenova , Mindju Thomas , Natalia Rey-Raap , Ana Arenillas , Francesco Lufrano , Antonia Stoyanova *

Posted Date: 23 November 2023

doi: 10.20944/preprints202311.1478.v1

Keywords: carbon xerogel; activated carbon YP-50F; Aquivion electrolyte membrane; solid-state supercapacitor; long lifetime

Article

Electrochemical Performance of Symmetric Solid-State Supercapacitors Based on Carbon Xerogel Electrodes and Solid-Polymer Electrolytes

Boryana Karamanova [1], Emiliya Mladenova [1], Mindju Thomas [2], Natalia Rey-Raap [3], Ana Arenillas [3], Francesco Lufrano [2] and Antonia Stoyanova [1,*]

[1] Institute of Electrochemistry and Energy Systems, Bulgarian Academy of Sciences, G. Bonchev Str. 10, 1113 Sofia, Bulgaria
[2] CNR-ITAE, Istituto di Tecnologie Avanzate per L'Energia "Nicola Giordano", 98126, S. Lucia, Messina, Italy
[3] Instituto de Ciencia y Tecnología del Carbono, INCAR-CSIC, Francisco Pintado Fe, 26, 33011, Oviedo, Spain
* Correspondence: antonia.stoyanova@iees.bas.bg

Abstract: Flexible energy storage devices, such as solid-state supercapacitors, are becoming increasingly attractive due to their characteristics of high electrochemical performance, reliability, light weight, flexibility, absence of electrolyte leakage, high power density, and long lifetime. For the optimization of the solid-state symmetrical supercapacitor proposed in this work, it was employed in sodium and lithium form Aquivion electrolyte membrane, which serves as the separator and electrolyte. As electrode materials, carbon xerogels, synthesized by microwave-assisted sol-gel methodology, with designed and controlled properties were obtained. Commercial activated carbon (YP-50F, 'Kuraray Europe' GmbH) was used for comparison. Specifically, the developed solid-state symmetrical supercapacitors deliver sufficient high specific capacitances of 105−110 F g^{-1} at 0.2 A g^{-1}, along with an energy density of 4.5 Wh kg^{-1} at 300 W kg^{-1}, and in a voltage window of 0-1.2 V in an aqueous environments, also demonstrating excellent cycling stability up to 10,000 charge/discharge cycles. These results can demonstrate the potential applications of carbon xerogel as an active electrode material and cation exchange membrane as the electrolyte in the development of solid-state supercapacitor devices.

Keywords: carbon xerogel; activated carbon YP-50F; Aquivion electrolyte membrane; solid-state supercapacitor; long lifetime

1. Introduction

Supercapacitors bridge the gap between traditional dielectric capacitors and batteries by providing several orders of magnitude higher energy density than dielectric capacitors and possessing higher power density and longer cycle life than batteries [1]. Flexible energy storage devices such as solid-state supercapacitors are becoming the most attractive electrochemical energy systems due to their flexibility, wear resistance, mechanical properties, low weight, no electrolyte leakage, etc. [2]. However, the flexibility and safety of supercapacitors have become key factors that place higher demands on researchers, and developing such devices with better electrochemical performance is still a huge challenge for them [3].

Each component of a supercapacitor (separator, electrode and electrolyte) has a significant influence on its electrochemical performance [4]. The properties of electrode materials and their physical structures directly determine the overall capacitive performance of this system [5]. This requires that the electrode material has a larger specific surface area and is in contact with the electrolyte to the greatest extent possible, to improv the electrochemical efficiency of the device [6].

Various porous carbon materials are widely used as electrode material in supercapacitor systems, and carbon aerogels and xerogels are considered a promising alternative due to their good

properties, such as electrical conductivity, high specific surface area, three-dimensional porous structure, and the ability to control pore size distribution.

Carbon gels are promising materials for energy applications due to a number of their interesting characteristics, such as: unique three-dimensional nano-lattice, porous structure, high electrical conductivity and controlled properties [7]. The specific surface area of organic xerogels is usually low (about 200 m^2g^{-1}), but its value can increase up to 600-700 m^2g^{-1} after the pyrolysis step under certain operating conditions [7,8]. By chemical activation, the microporosity of the material can be further increased to surface area values of almost 2000 m^2g^{-1} [9,10]. Many factors are involved in this process, which makes it possible to design the porosity of carbon xerogels by selecting specific activation parameters, such as the activation agent and precursor used, activation temperature and time, etc [10,11]. All these indicate the great potential for obtaining carbon xerogels with controlled micro/mesopores and the influence of synthesis conditions on their energy storage capacity.

The research and development of flexible solid polymer electrolyte membranes has been the subject of increased interest in recent years. These membranes must have good ionic conductivity to ensure efficient operation of the supercapacitor. Research and development of less explored but effective ion exchange membranes for supercapacitors (e.g. proton exchange membranes (PEM) and anion exchange membranes (AEM)) also require improved scalable synthesis techniques, fabrication techniques and understanding of fundamental physical processes. The development of high-performance flexible supercapacitors relies heavily on innovative materials that have good electrical and mechanical properties [12]

The effect of the interaction between the electrodes and the electrolyte is also an important factor, and understanding the interactions between them is essential in designing more efficient electrode materials. In addition, it is known that the electrochemical behaviors of the electric double layer electrodes are decided not only by the exposed surface area of the carbon electrode, but also by the matching degree between the pore size distribution of carbon electrode and the size of solvated ions in the electrolytes [13,14].

Numerous studies have been conducted on supercapacitors using aqueous electrolytes based on lithium or sodium sulfate [15,16]. The choice of the cation has been determined by investigating sulfate salts with different alkali metal cations (such as Li^+, Na^+ and K^+) and their influence on the electrochemical characteristics of these systems [17,18]. An advantage is that sulfates can be applied not only as liquid state electrolytes but also as gel electrolytes [19]. The economic aspect is also very important, considering that Li_2SO_4 and Na_2SO_4 are the cheapest among the alkali metal sulfate salts [20].

The best results obtained for an aqueous solution of Li_2SO_4 are explained by the ion sizes. In aqueous solution, the alkali metal ions are highly dissolved and the diameter of the ion-solvent complex increases in the order $K^+ < Na^+ < Li^+$. The highest capacitance values obtained for the largest and most dissolved ions are due to their low mobility and low diffusion coefficient. Na^+ and K^+ cations are characterized by a smaller ion–solvent complex diameter and are have a higher mobilities and diffusion coefficients, also their solvation/ desolvation energy, therefore they can be sorbed differently in the micropores [17]. The result obtained can be explained by the fact that in EDLC very high ion mobility is not required for charging and discharging the double electric layer, in contrast to pseudocapacitive systems where fast redox processes require fast ion transfer at the electrode/electrolyte interface [17].

In the development of supercapacitors, it should also be foreseen that the selection of separators with better performance has a decisive impact on the integration of their overall performance [21].

The aim of this work is synthesis of nano-structured carbon xerogels by microwave-assisted sol-gel methodology with designed and controlled properties and their use in the electrode preparation and fabrication of symmetric solid-state supercapacitors. For their optimization it is proposed Na^+- and Li^+- form Aquivion® E87-05S electrolyte membrane, that serves as separator and electrolyte. The assessments of the electrochemical characteristics were performed by cyclic voltammetry (CV), galvanostatic charge/discharge measurements, electrochemical impedance spectroscopy (EIS) and long-term tests. The capacitance performances of the obtained carbon xerogels were compared to

 doi:10.20944/preprints202311.1478.v1

those of a commercial activated carbon (YP-50F, "Kuraray Europe" GmbH) in order to establish the structural and surface characteristics of carbon materials that may influence the performance of solid-state supercapacitors.

2. Results and Discussion

2.1. Physical Chemical and Morphological Characterizations of Carbons

The activated carbon xerogel obtained is a synthetic carbon with no impurities and low content of oxygen. Table 1 shows the elemental analysis of the activated carbon xerogel (AX) and the commercial carbon used for comparative purposes. As can be observed the chemical composition of both carbons is very similar, mainly composed by carbon.

Table 1. Elemental analysis of the carbon xerogel synthetized and the commercial carbon YP-50F.

Sample	C (wt%)	H (wt%)	O (wt%)	N (wt%)	S (wt%)
AX	96.3	0.7	3.0	-	-
YP-50F	97.6	0.3	2.1	-	-

Although the two carbons did not differ substantially from a chemical point of view the different nature of the carbons may influence on their further interaction with electrolytes. There is not a specific measurement to analyze such interaction, but the wetting angle could be used to evaluate the interaction of the electrodes surface and the electrolytes evaluated. Therefore, the wettability of AX and YP-50F, as part of their electrodes, versus Na_2SO_4 and Li_2SO_4 electrolytes were measured and the results showed in Figure 1.

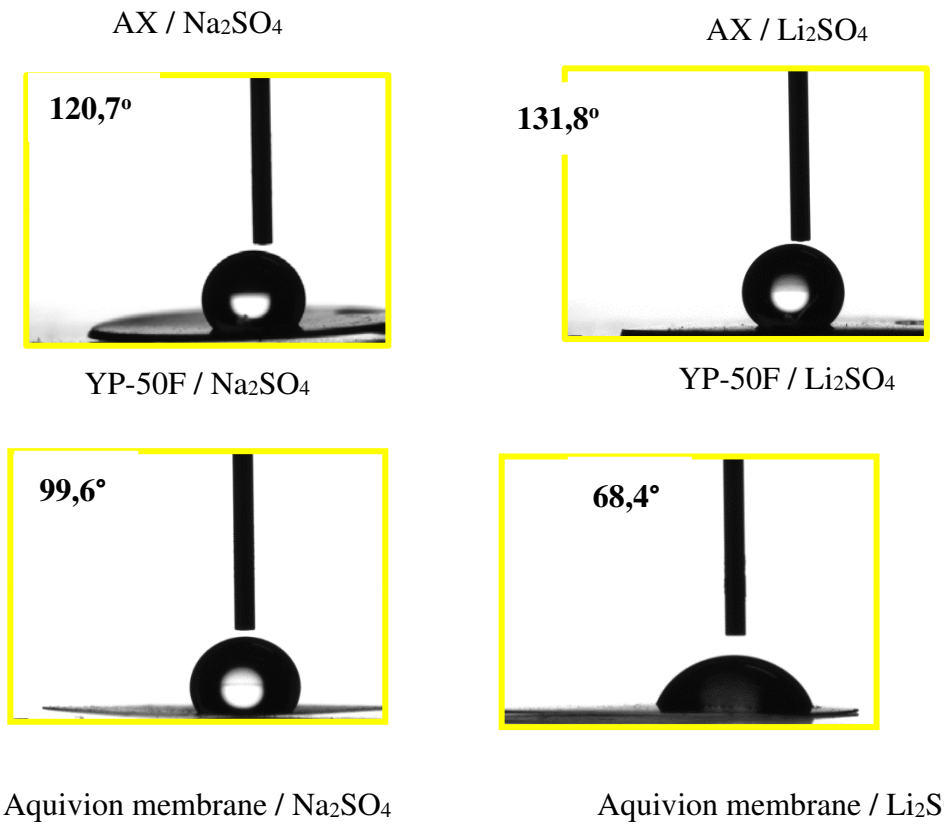

Preprints (www.preprints.org) | NOT PEER-REVIEWED | Posted: 23 November 2023 doi:10.20944/preprints202311.1478.v1

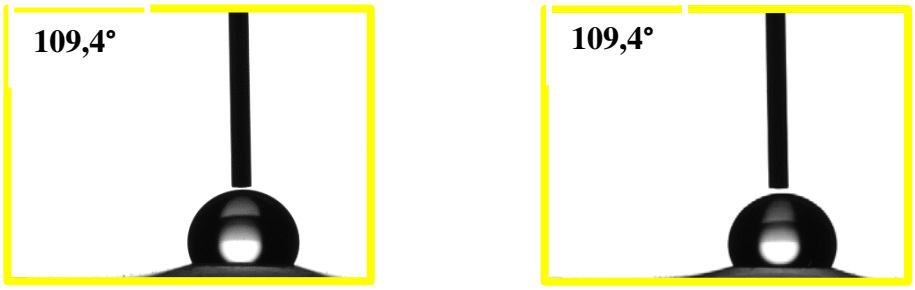

Figure 1. Electrode wetting angles of the electrodes made of AX and YP-50F, besides the Aquivion membrane versus Na_2SO_4 and Li_2SO_4 (both 1M).

It was observed that whilst the Aquivion membrane shows no differences in the wettability to both electrolytes (Na_2SO_4 and Li_2SO_4) there are clear differences in the wettability of the carbons. The activated carbon xerogel exhibited better wettability with Na_2SO_4 than with Li_2SO_4, whilst YP-50F shows the opposite, with a clear affinity to Li_2SO_4. This could be very relevant in their further electrochemical behavior in the cell.

Both carbons were also characterized by SEM and Figure 2 shows a clear difference also in the surface morphology.

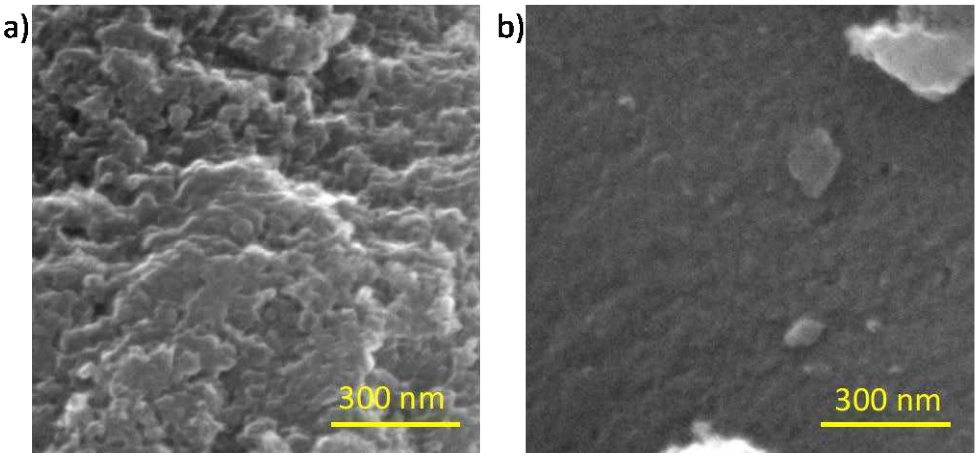

Figure 2. SEM photographs of carbon AX obtained by sol-gel process in this work (a) and the commercial carbon YP-50F.

As can be observed in Figure 2, the morphology at nanoscale is also very different between both samples. The AX shows higher surface roughness and some clear feeder pores are observed. On the contrary, YP-50F shows no roughness and the present porosity should be narrower than in the activated carbon xerogel.

In order to analyze the porosity of both samples, the N_2 adsorption-desorption isotherms were performed. Isotherms are presented in Figure 3 and the main porous parameters are summarized in Table 2.

Preprints (www.preprints.org) | NOT PEER-REVIEWED | Posted: 23 November 2023 doi:10.20944/preprints202311.1478.v1

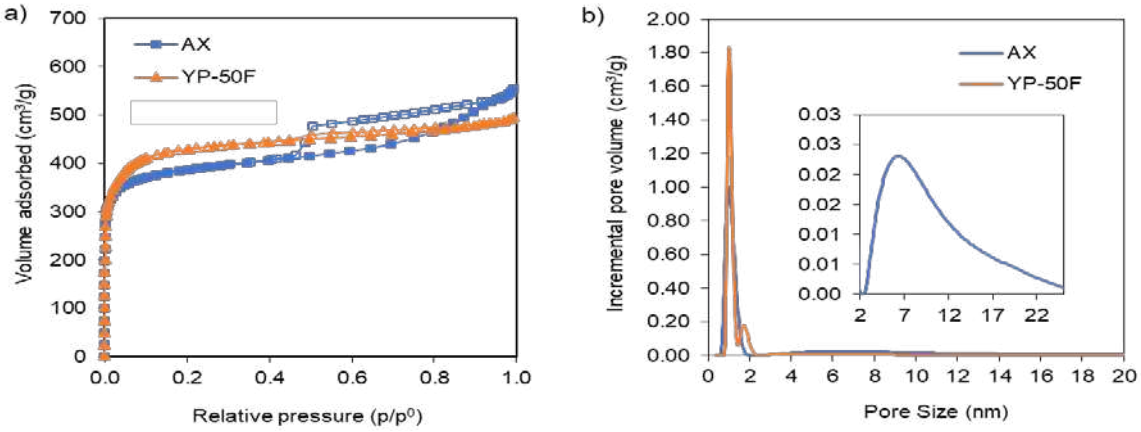

Figure 3. N_2 adsorption-desorption isotherms (a) for the carbon samples studied and their pore size distribution (b) according to the NLDFT model.

Table 2. Main porous parameters for the carbon xerogel AX and the commercial carbon YP-50F obtained from N_2 adsorption: specific surface area (S_{BET}), external surface area (S_{ext}), micropore volume (V_{micro}) and total pore volume (V_t).

Sample	S_{BET}, m^2g^{-1}	S_{ext}, m^2g^{-1}	V_{micro}, cm^3g^{-1}	Vt, cm^3g^{-1}
AX	1492	234	0.59	0.85
YP-50F	1756	157	0.62	0.80

Both carbons have high volume of microporosity as can be observed in Table 2. The microporosity is quite close between samples although the commercial YP-50F has slightly higher micropore volume and therefore higher specific surface area. The total volume of pores (V_t) is also very close between both samples. However, observing the N_2 isotherms, showed in Figure 3, the shape is a bit different indicating a different porous structure as was previously expected from the SEM micrographs. YP-50F isotherm is type I characteristic of microporous samples, with a high increase in the volume adsorbed at low relative pressures and then no increase of the adsorption. On the other hand, the activated carbon xerogel AX presents an increase of the volume adsorbed at low relative pressures indicating the presence of microporosity, but then there is a constant increase of the volume adsorbed in the whole range of pressures with the typical presence of a hysteresis loop indicating the existence of mesorporosity. Applying the NLDFT method to the adsorption data, a pore size distribution can be obtained (Figure 3b). It can be observed that YP-50F is just a microporous sample, with pores < 2nm exclusively, whilst AX has micropores and feeder pores centered in 10 nm, as was expected from the sol-gel synthesis conditions.

Therefore, although the chemical analysis is very similar between both samples (AX and YP-50F) some differences in wettability versus the electrolytes were detected. On the other hand, although both samples present microporosity and very close surface area values, it is clear that different porous structure is present in both samples. The presence of feeder pores in the case of AX may influence on diffusional aspects, in fact the external surface area is quite higher in the case of AX sample. This could influence in the electrode conformation and the further behavior in the supercapacitor cell.

2.2. Electrochemical Characterization of Symmetric Supercapacitors

Several methods have been applied to study the electrochemical characteristics of activated carbon xerogel (AX) more precisely. The supercapacitor cells were investigated under identical experimental conditions, allowing comparison with commercial carbon (YP-50F) as well as between the two electrolytes (Na^+ and Li^+ exchange membrane). To follow the changes that occurred in the

Preprints (www.preprints.org) | NOT PEER-REVIEWED | Posted: 23 November 2023 doi:10.20944/preprints202311.1478.v1

electrode, CV- curves and EIS were recorded at the beginning of the experiment and after galvanostatic charge/discharge at different current loads (100 to 1,000 mAg^{-1}) and a long cycle test (10,000 cycles at 200 mAg^{-1}).

Figure 4 compares the voltammograms of AX and YP-50F cycling in lithium and sodium based polymer electrolyte membranes. In general, all voltammograms are typical for symmetric supercapacitor systems with almost rectangular shapes and almost overlapping each other when the scan rate is increased from 10 to 50 mVs^{-1}. The rectangular shape of the voltammograms is maintained without any distortion even at high scan rate, suggesting excellent capacitive behavior of the devices [22].

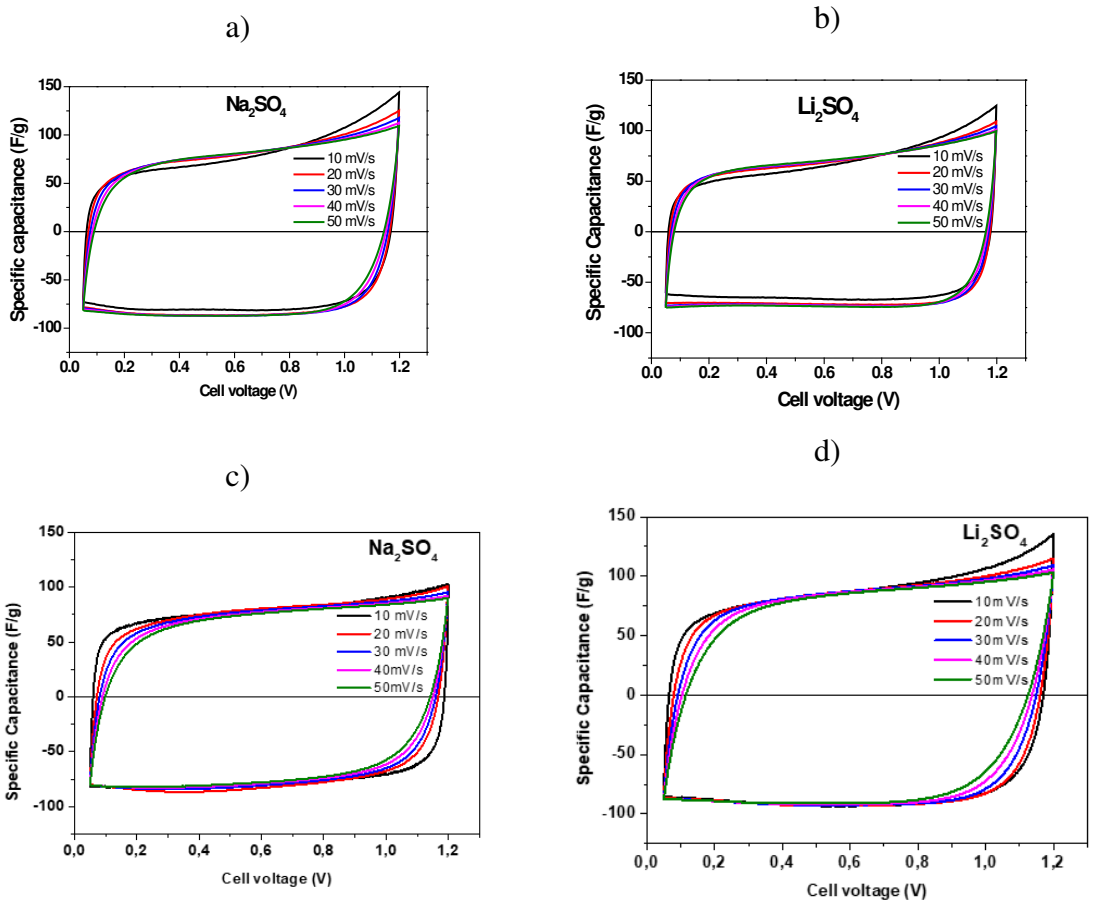

Figure 4. Cyclic voltammogram carried out from 10 to 50 mVs^{-1} in the voltage range from 0.05 to 1.2 V using Na^+ and Li^+-form of Aquivion membrane with AX (a,b) and YP-50F (c,d).

To further distinguish the characteristics of AX and YP-50F in lithium and sodium electrolytes, galvanostatic charge/discharge tests were conducted. For a better comparison, their calculated discharge capacitances (according to Eq. 2) and their dependence on discharge current density are compared in Figure 5.

There are several points that need to be outlined. The specific capacitance decreases with increasing current density, probably due to the remarkable enhancement of the diffusion limitation inside the deeper pores [23]. This capacitance decline is most pronounced for cell with activated carbon xerogel (AX) and Na^+-exchange membrane. The comparison of GCD curves reveals also that the capacitances are higher in both cases for Li^+-electrolyte than Na^+. This result correlates well with studies in aqueous solutions, according to which the better performance of Li_2SO_4 compared to Na_2SO_4 and K_2SO_4 in symmetric supercapacitors is due to their low mobility and low diffusion coefficient (charge/discharge of EDLC does not require very high ion mobility) [17,24]. Electrochemical tests conducted in 6 M NaOH, KOH and LiOH alkaline electrolytes on two active

Preprints (www.preprints.org) | NOT PEER-REVIEWED | Posted: 23 November 2023 doi:10.20944/preprints202311.1478.v1

carbons (YP-50F and YP-80F) show that their capacitive characteristics are a consequence of both the different conductivity of the electrolyte and the interaction between the electrolyte and the functional groups of the electrode material. For example, the capacitance of YP-50F was found to improve in the following order: NaOH < LiOH < KOH, while for YP-80F the order changed to LiOH < NaOH < KOH [25].

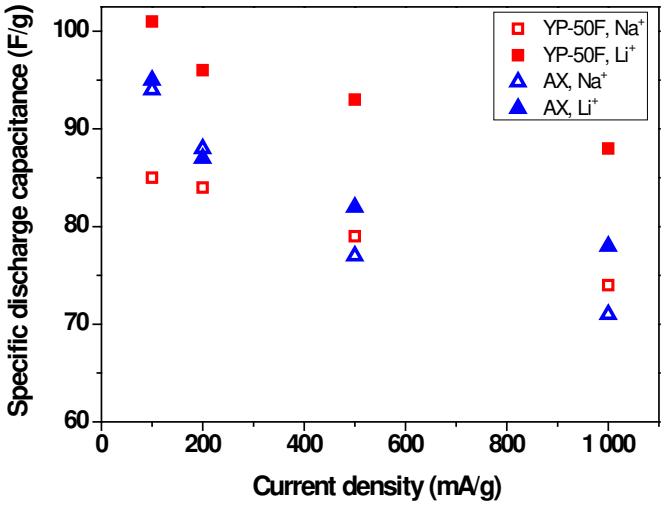

Figure 5. Galvanostatic charge/discharge curves as a function of the current load for symmetric supercapacitors with AX-1500 and YP-50F using Na^+- and Li+-form of Aquivion membrane.

On the other hand, the results in Fig. 5 show that YP-50F has better initial capacitance than AX, and this result can be related to the different pore textures and wetting angle mentioned above. It is found that the pore size distribution of carbon materials can affect the access of electrolyte ions to the electrode surface, which influences the capacitance and rate capability of the system [26]. Zhao et al. suggested that the effects of surface wettability affect the thermodynamic and dynamic properties, and it can be improved by controlling the surface functional groups of the carbon material [27].

YP-50F shows much better wettability than the carbon xerogel, especially in Li_2SO_4 (Fig. 1), and therefore better surface wettability with this electrolyte, which is one of the possible reasons for the obtained highest initial capacitance. On the other hand, the different surface morphology of the two carbons determines their different capacitive behaviour. To explain the results obtained, it should also be kept in mind that YP-50F is only a microporous sample with pores < 2 nm and this means that all pores of YP-50F are likely accessible to the alkali ions. AX has micropores and feed pores and therefore a much larger external surface area which affects ion diffusion.

2.3. Long-Term Durability of Investigated Supercapacitors

The characteristics of carbon electrodes with Na^+ and Li^+ -form Aquivion membranes were further studied based on their cycling stability (Figure 6). Long-term testing includes 10,000 charge and discharge cycles at a current load of 200 mAg^{-1}. In general, AX and YP-50F demonstrate excellent cycling stability in both electrolytes (less than 3-4% of variability in specific capacitance after 10,000 cycles). These results are well shown from high Coulombic efficiencies as reported in Table 3. A low initial efficiency of the capacitor based on AX and Li^+-Aquivion membrane is to ascribed at low wettability of the carbon. This probably means that the ionic conductivity of the electrolyte and the ionic sizes of Li^+ and Na^+ are not the only factors that contribute to the performance of the supercapacitor [25].

Preprints (www.preprints.org) | NOT PEER-REVIEWED | Posted: 23 November 2023 doi:10.20944/preprints202311.1478.v1

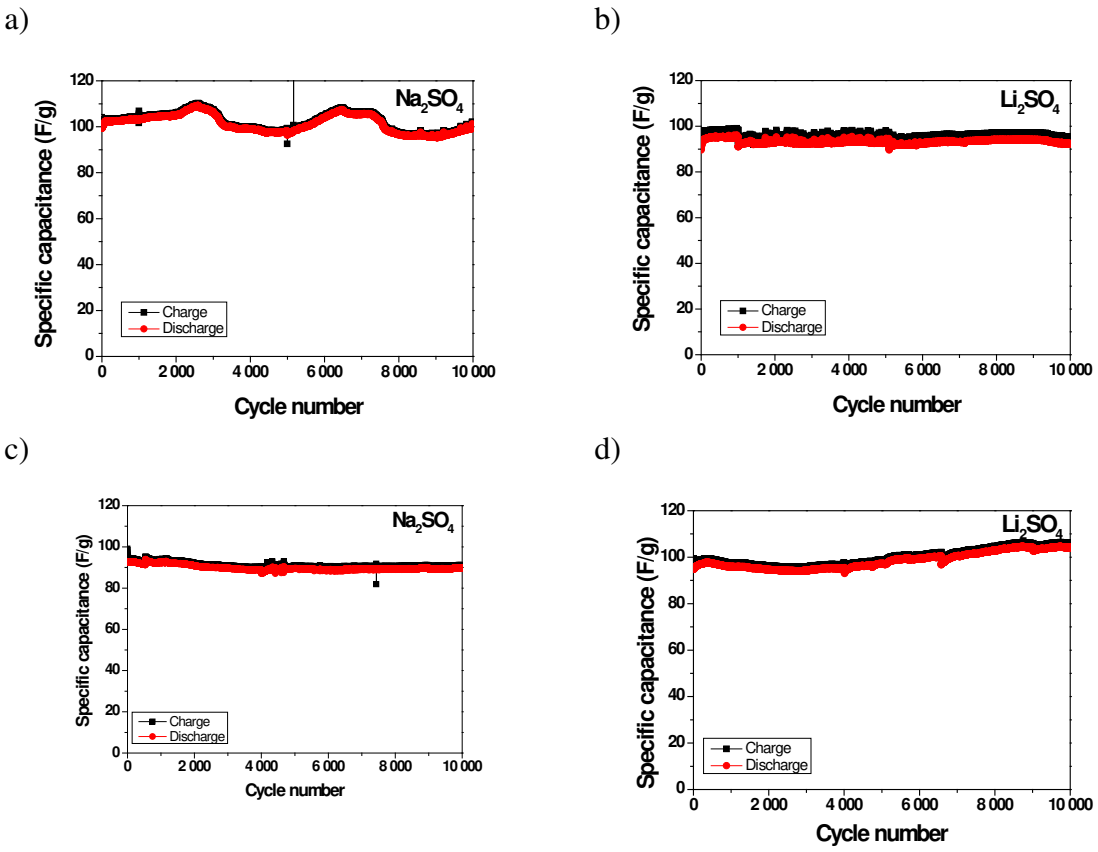

Figure 6. Long-term tests at 200 mAg^{-1} for symmetric supercapacitors with AX (a,b) and YP-50F (c,d) using Na^+- and Li^+-form of Aquivion membrane.

Table 3. Coulombic efficiency after various cycles .

Coulombic	1st cycle		after 1 000 cycles		after 5 000 cycles		after 10 000 cycles	
efficiency, %	Na_2SO_4	Li_2SO_4	Na_2SO_4	Li_2SO_4	Na_2SO_4	Li_2SO_4	Na_2SO_4	Li_2SO_4
AX	96	82	99	97	99	97	99	97
YP-50F	94	95	99	98	99	98	99	98

After the completing 10,000 cycles, the best electrochemical performance is observed for YP-50F electrodes operating in Li_2SO_4 electrolyte, with a capacitance 105 Fg^{-1} and a Coulombic efficiency - over 98% (Table 3 and Figure 7). It can also be found that the AX sample exhibits higher capacitance than the YP-50F in the Na_2SO_4 electrolyte 99 Fg^{-1} vs. 89 Fg^{-1} after 10,000 charge-discharge cycles. This result corresponds well with that shown in Figure 5. A possible reason for this is the dominant influence of the conductivity of the Na^+-electrolyte, as well as the ongoing interactions between it and the carbon electrode during the continuous cycle.

Preprints (www.preprints.org) | NOT PEER-REVIEWED | Posted: 23 November 2023 doi:10.20944/preprints202311.1478.v1

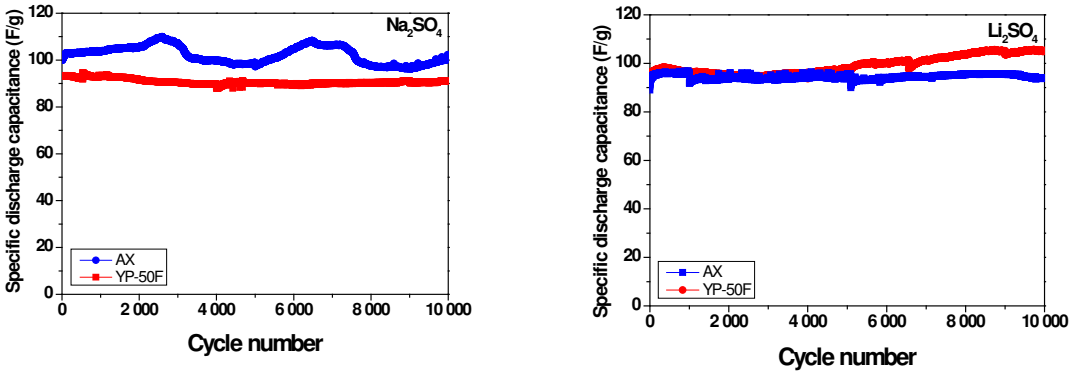

Figure 7. Long-term tests at 200 mAg^{-1}.

After 1,000, 5,000, and 10,000 galvanostatic charge/discharge cycles, CV curves were recorded for each supercapacitor, shown in Fig. 8 at 10 mVs^{-1}. As can be seen, the rectangular shapes for all supercapacitors remain unchanged, with a slight area shrinkage observed. This result confirms the very excellent stability of these designed solid-state supercapacitors.

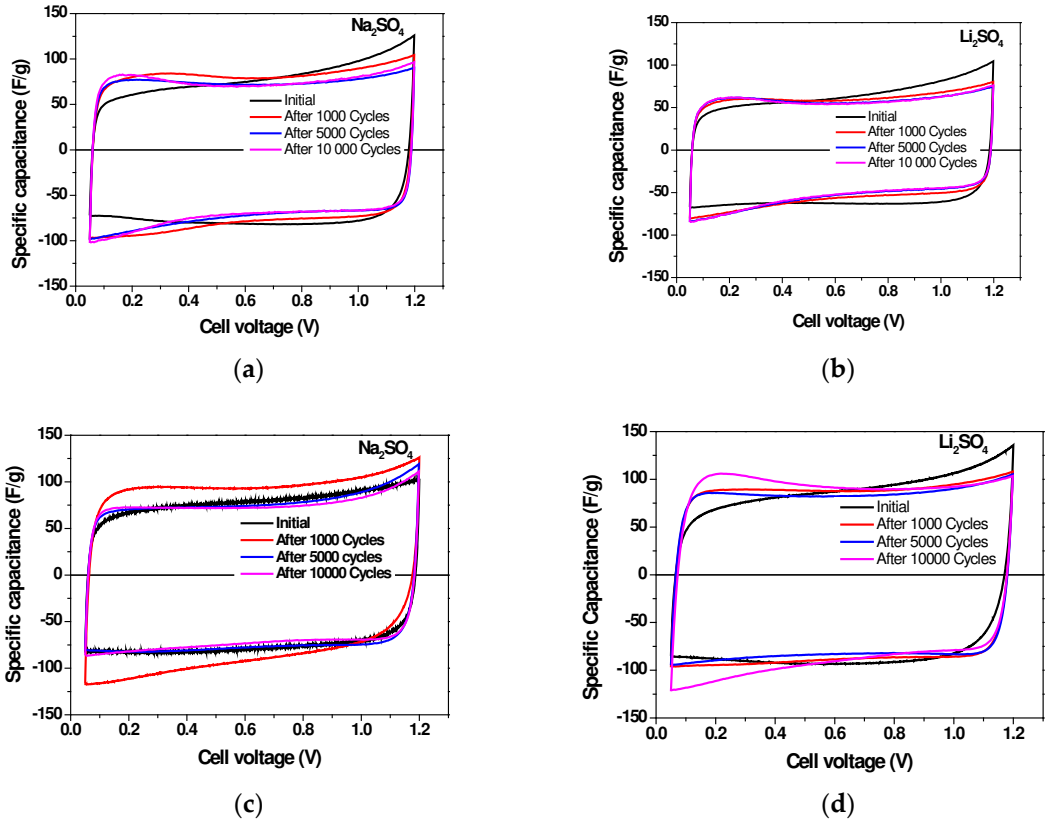

Figure 8. Cyclic voltammogram carried out at 10 mVs^{-1} in the voltage range from 0.05 to 1.2 V using Na^+ and Li^+-form of Aquivion membrane with AX (a,b) and YP-50F (c,d) after 1000, 5000 and 10000 cycles.

Furthermore, electrochemical impedance spectroscopy (EIS) was also carried out to elucidate the impedance features of various supercapacitors at begin of tests and after 10,000 cycles. Nyquist plots for the different capacitors are presented in Fig. 9a and 10a. The internal resistance of electrolyte membranes (R_s, the lower Z′ value with imaginary impedance (Z′′) > 0) values of the resultant

Preprints (www.preprints.org) | NOT PEER-REVIEWED | Posted: 23 November 2023 doi:10.20944/preprints202311.1478.v1

demonstrate high Li^+- and Na^+ -ions conductivities, with values of 7.9 and 6.8 $mScm^{-1}$ for Na^+-form and Li^+-for Aquivion electrolyte membranes, respectively. These values for solid electrolytes are lower than the proton conductivity of the Aquivion membrane [28] at room temperature that are ranging from 120-160 $mScm^{-1}$ [28,29]. From the Nyquist plots, it is also noted that supercapacitors with YP-50 show a semicircle of different radius, due to an additional charge transfer resistance (R_{ct}) that probably arises from a secondary resistance for some faradic process occurring in the electrodes or due to electrode/current-collector interface resistances [29,30]. The first possibility in these spectra seems to be less likely because they are not present for all SCs with AX-1500, even after tens of thousands of cycles. This improved behavior is confirmed in Fig. 9d and 10d, which shows the increases of capacitance as the frequency decreases for both capacitors using Na^+ and Li^+-form Aquivion electrolyte membrane. However, in these graphs (Figs. 9 and 10) it is shown that the specific capacitance also increases at the end of the stability cycles, which is not an obvious finding, but is probable that during the progression of the stability tests an increased penetration and then wetting of ions (i.e. Na^+, Li^+) in the narrow pores may occur slowly with the help of hydrophilic carbon oxygen groups, as clearly shown in Figs. 9b-10b. This latter are highlighted as the resistance decreased as the stability tests proceed, and their values are lower after 10,000 cycles for the same capacitor, confirming this explanation.

A further very excellent result shown by the EIS analysis is well evidenced from the trend of phase shifts (phase angle), which are always ≥ to -83 degrees (i.e. (-) 83-88°) for all capacitors and in particular the phase angles are even higher at final stability tests as can be seen in the Bode plots of Figs. 9c-10c.

The phase shift values greater than -83° further support the fact that in these supercapacitors there is no evidence of strong faradic reactions [31] as one might think from the semicircles in the Nyquist plot inset of Figures 9a-10a. Therefore, it is demonstrated that the appeared semi-circles (in inset of Figures 9a-10a) are to assign at interfacial electrical contact resistances.

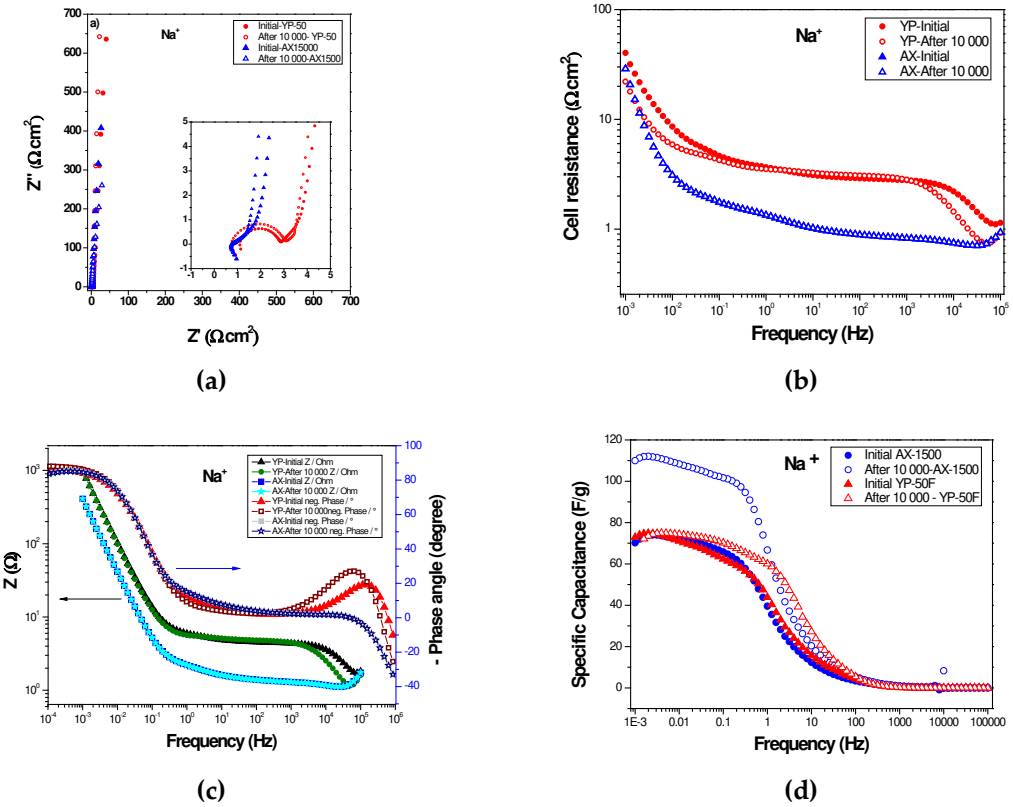

Figure 9. EIS of SC with AX and YP-50F and Na^+-exchange Aquivion membrane before and after 10 000 cycles: a) Nyquist plots (the inset shows the high frequency region), b) cell resistance as a function of the frequency, c) Bode plots, d) Specific capacitance as a function of the frequency.

Preprints (www.preprints.org) | NOT PEER-REVIEWED | Posted: 23 November 2023 doi:10.20944/preprints202311.1478.v1

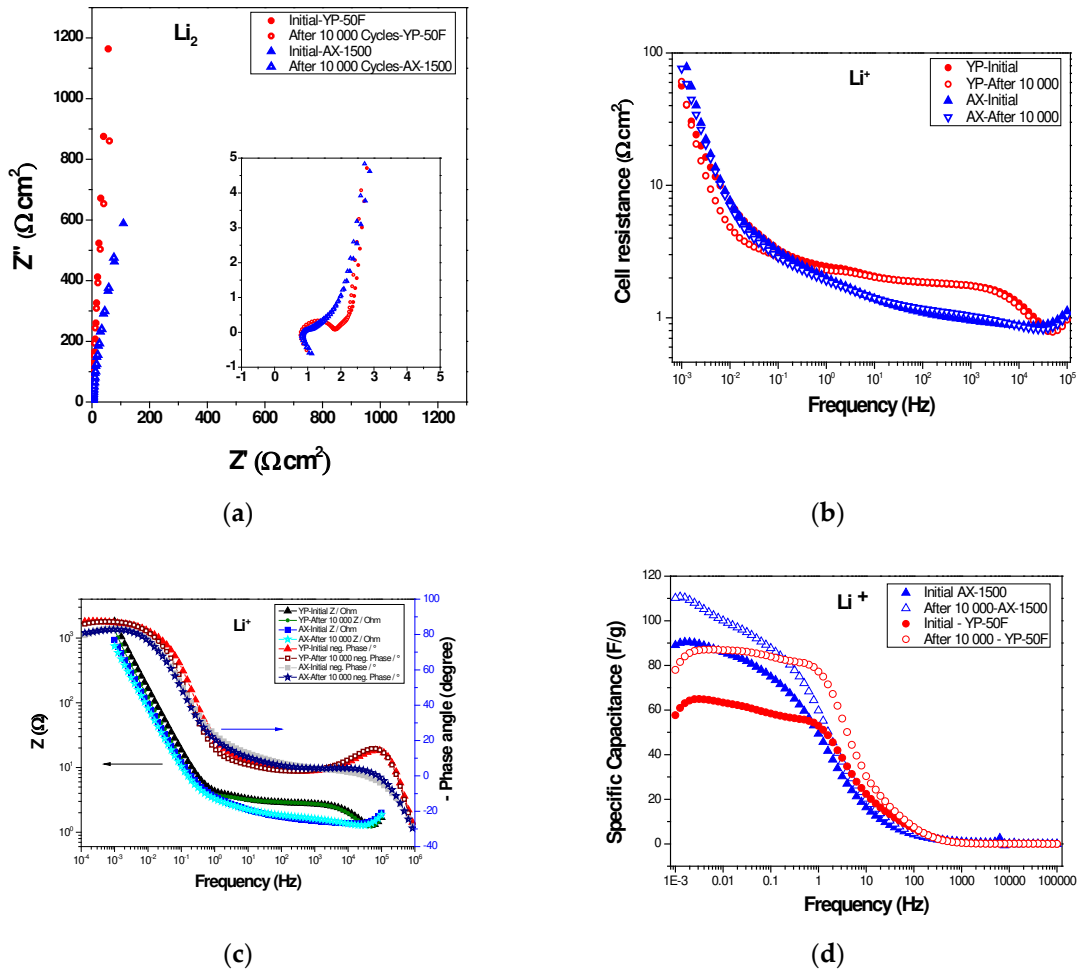

Figure 10. EIS of SC with AX and YP-50F and Li^+-exchange Aquivion membrane before and after 10 000 cycles: a) Nyquist plots (the inset shows the high frequency region), b) cell resistance as a function of the frequency, c) Bode plots, d) Specific capacitance as a function of the frequency.

The electrochemical characteristics of the studied carbons were evaluated by Ragon plots for all supercapacitor cells in both electrolytes (Fig. 11). The data in the figure show that YP-50F in Li_2SO_4 provides a specific energy density of 4.5 Wh kg^{-1} at a power of 50 Wkg^{-1} and maintains a relatively constant value of 4.0 Wh kg^{-1} even at a power density of 330 Wkg^{-1}. Although these values obtained are relatively low, they are the highest compared to SC cells shown in Fig. 11. In comparison, AX exhibits an energy density of 3.6 Wh kg^{-1} at a power density of 330 Wkg^{-1} when applied as an electrode in a Li_2SO_4 supercapacitor. The energy density of the supercapacitor using Na^+-form Aquivion membrane is lower.

Preprints (www.preprints.org) | NOT PEER-REVIEWED | Posted: 23 November 2023 doi:10.20944/preprints202311.1478.v1

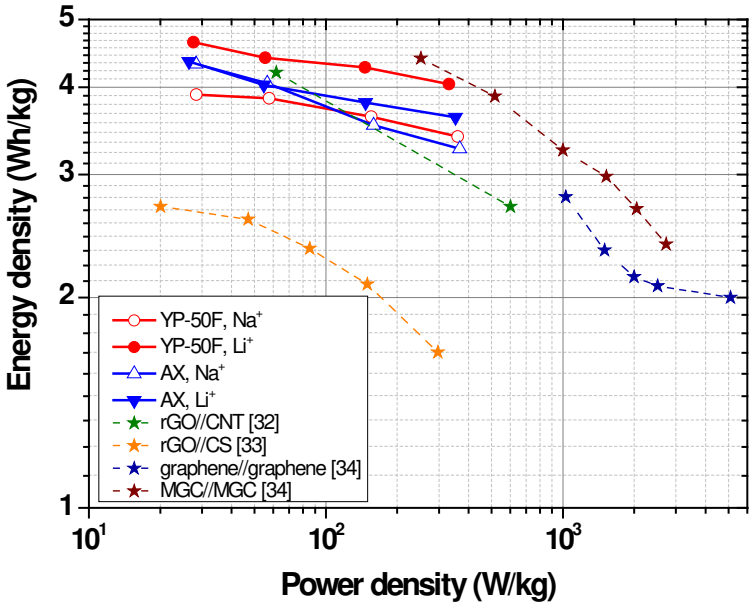

Figure 11. Energy density versus power density (Ragone plot) for SCs with AX and YP-50F and Na^+ and Li^+- exchange Aquivion membrane. Literature results reported [32], [33], [34] are presented for comparison.

3. Conclusions

A carbon xerogel with designed and controlled properties was synthesized by microwave sol-gel methodology and investigated as an electrode material in the development of solid-state symmetric supercapacitors. The studies were conducted using Na^+- and Li^+- form Aquivion electrolyte membranes. Commercial activated carbon YP-50F was used to produced carbon electrodes and fabricate supercapacitors for comparison. The synthesized carbon xerogel exhibits good electrochemical performance, with low resistance and also very excellent cycle stability up to 10,000 charge-discharge cycles.

Furthermore, the study shows that both YP-50F and AX can be considered as suitable electrode materials for the development of solid-state supercapacitors with excellent electrochemical performance in both Li^+ and Na^+ form of polymer electrolyte membranes. These results indicate that the electrochemical performance depends not only on the ion conductivity of the electrolyte but also on the size of Li+ and Na+ ions and their electrode wettability. In addition, the external surface area of AX is larger than that of YP-50F activated carbon and probably affects the diffusion process, while the different pore structure and wettability of electrode materials influence the capacitive properties of the supercapacitor. The interaction between the functional groups of the carbons and the cations in the polymer membrane are also factors to be considered to elucidate the resulting effect.

It is demonstrated that the devices studied can operate with a good voltage window of 1.2 V and exhibit a specific capacitance between 105 and 110 F g^{-1} at 0.2 A g^{-1}, which corresponds to an energy density of 4-4.5 Wh kg^{-1} at 300 W kg^{-1}. Such good electrochemical performance could be attributed to the following reasons: 1) the good textural characteristics of the carbon xerogel (AX); 2) the design of the cell configuration using Na^+ and Li^+ exchange Aquivion electrolyte membranes, which provide high ionic conductivities as well as high electrochemical utilization and tight sealing after being sealed in the cells; and 3) the polymer electrolyte can prevent the leakage of the sulfate electrolyte, which offers the possibility of assembling into potential foldable devices.

 doi:10.20944/preprints202311.1478.v1

4. Experimental

4.1. Synthesis of Carbon Xerogels

Sol gel methodology was employed to obtain a synthetic carbon with very well controlled physicochemical properties. Resorcinol $C_6H_6O_2$ (Indspec, 99.6% purity) and formaldehyde CH_2O (Merck,37% aqueous solution) were used as precursor monomers and they were dissolved in water, that was used as the reaction media. The initial pH of the precursor mixture was around 3 and it was raised to 6.5 with NaOH in order to promote the polymerization reaction and to obtain a polymeric structure with a mean pore size ca. 10 nm, according to previous works [35,36]. To promote the sol-gel process it is necessary to heat the mixture to a temperature always below 100ºC. In this case the precursors were heated at 85ºC by means of microwaves. This particular way of heating is a very simple, safe and quick method to heat aqueous samples, and in this case it provides great advantages such as the short process time (i.e. 5 h) and the use of just one single device for the whole process (i.e. nucleation, crosslinking, curing and drying the gel), in comparison with the traditional methodologies. The temperature in the microwave was controlled with a thermocouple introduced in the precursor mixture and connected to a PID controller that adjust the power of the magnetron and the pulses to maintain the operating temperature (85ºC) constant. After 5 hours the solid and dried polymer obtained underwent a post-synthesis treatment at 1000ºC under CO_2 flow. This treatment produces two types of changes in the polymer: (i) devolatilization process because of the heat treatment up to 1000ºC, where all labile functional groups (i.e. mainly oxygen groups) are removed and the sample elemental composition is concentrated in carbon; and (ii) activation process due to the presence of CO_2 as reactant, where defects are produced in the carbon structure due to the partial gasification of the carbon structure with the oxidant reactant. These defects are mainly micropores, and they are created inside the nodules of the polymer, whilst the feeder pores of 10 nm created during the sol-gel process remain intact and they are located between nodules. Therefore, at the end of the process an activated carbon xerogel (AX) is created with no impurities, mainly composed by carbon (>95 wt%C), with feeder pores of 10 nm and high volume of microporosity that would provide high surface area.

4.2. Physicochemical Characterization of Carbon Xerogels

The carbon xerogel obtained was characterized by different techniques in order to have information about its chemical composition, morphology and porous properties. The commercial activated carbon YP-50F from Kuraray Europe was also characterized for comparative purposes.

Elemental analysis, C, H and N contents, of the samples were measured in a LECOCHNS-932 microanalyzer, while the O content was determined in a LECO-TF-900 device. Both samples present no impurities content. The surface chemical composition may influence in the interaction with electrolytes, and more specifically in the wetting behaviour of the samples. Therefore, wetting angle was measured on an apparatus Force Tensiometer K100 of KRÜSS K100. The measurement consists in dropping of 10 µl of the solution on the electrode made with the sample to study, and observe the shape of the drop to obtained the value of the wetting angle. This measurement was performed 5 times in order to have an averaged value per electrode.

The morphology of the samples was observed by scanning electronic microscope, SEM (Quanta FEG 650 microscope), while the porous properties were evaluated by N_2 adsorption-desorption isotherms at 77K (Micromeritics Tristar II). Samples were outgassed overnight at 120ºC before analysis. From these isotherms the textural parameters such as specific surface area and micropore volume can be obtained from BET equation and NLDFT method. The total pore volume was obtained from the total amount of nitrogen adsorbed at the saturation point (i.e. P/P0=0.99).

 doi:10.20944/preprints202311.1478.v1

4.3. Preparation of the Carbon Xerogel Electrodes

The composition of the prepared electrodes was 80 wt.% of the activated carbon xerogel, 10 wt. % poly-(vinylidene fluoride-co-hexafluoropropylene) and 10 wt. % graphite fibers. The electrodes with activated carbon YP-50F, was prepared with the same procedure and used for comparison.

The electrodes were prepared by a casting technique. Poly (vinylidene fluoride-co-hexafluoropropylene) in grain form was dissolved in N,N-dimethylacetamide (3% solution) before the use. For good homogenization of the materials, they are mixed and stirred for 15 minutes. The layer with thickness of 500μm is formed on a glass-plate using Film Applicator Elcometer 4340 and was dried at 40°C for 5 h and 12 h at 70°C, then separated by distilled water and finally dried at 120 °C for 1 h.

4.4. Activation of the Polymer Electrolyte Membrane and Electrochemical Characterization

As electrolyte and separator was used Aquivion®E87-05S membrane, with an equivalent weight of 870 g mol^{-1} and a thickness of 50 μm, purchased from Solvay. The membrane was activated to the Na^+- and Li^+-form by immersion in 1 M Na_2SO_4 and 1 M Li_2SO_4 solution, respectively, for 24 hours at room temperature before being assembled in cell.

The activated Aquivion membrane with an area of 0.79 cm^2 and the carbon electrodes with the area of 0.64 cm^2 were mounted in a two-electrode coin Swagelok-type cell.

The electrochemical measurements on supercapacitors were performed using cyclovoltammetry (CV) at different scan rates that ranged from 10 to 50 mV s^{-1}, in the voltage range of 0.05–1.2V, using an Multi PalmSens system (model 4, The Netherlands). The electrochemical impedance spectroscopy (EIS) measurements were performed using a same apparatus at frequencies ranging from a 10 MHz to 1 mHz. The galvanostatic charge-discharge measurements were performed using an Arbin Instrument System BT-2000 in the range between 0.05 and 1.2 V. The test program was executed at a constant current load of 100 to 1 000 mAg^{-1} for 100 cycles per step. The cells were subjected to a long-term cycling tests at current rate of 200 mAg^{-1} for 10 000 cycles charge-discharge. The specific capacitance, Cs, obtained from cyclic voltammetry was calculated by:

$$Cs=[4(I/(dV/dt))/m] \quad (1)$$

where I is the current, dV/dt is the voltage scan rate, and m is the mass of the active carbon material.

The following equation was used to calculate the specific capacitance from the charge/discharge curves:

$$C= (4I\times\Delta t)/(m\times\Delta V) \quad (2)$$

where I (A), Δt (s), m (g) and ΔV (V) indicate discharge current, discharge time, mass of active material, and voltage window respectively.

On the basis of the specific discharge capacitance, the energy density (E) and power density (P) is calculated using equations 3 and 4:

$$E= C\,\Delta V^2 /7.2 \quad (3)$$

$$P = E/t \quad (4)$$

Acknowledgments: This research was carried out within the BIScaps project, which was supported by contract No. DO1-286/ 07.10.2020, funded by the Ministry of Education and Science of Bulgaria, to whom the authors express their gratitude. Some of the experiments were performed using equipment included in the National Infrastructure NI ESHER supported by the Ministry of Education and Science under grant agreement No DO1-160/28.08.18.

References

1. [1] M. M. Pérez-Madrigal, F. Estrany, E. Armelin, D. D. Díaz, and C. Alemán, "Towards sustainable solid-state supercapacitors: electroactive conducting polymers combined with biohydrogels," *J. Mater. Chem. A*, vol. 4, no. 5, pp. 1792–1805, 2016, doi: 10.1039/C5TA08680A.
2. [2] S. T. Senthilkumar, Y. Wang, and H. Huang, "Advances and prospects of fiber supercapacitors," *J. Mater. Chem. A*, vol. 3, no. 42, pp. 20863–20879, 2015, doi: 10.1039/C5TA04731E.
3. [3] W. Li, H. Lu, N. Zhang, and M. Ma, "Enhancing the Properties of Conductive Polymer Hydrogels by Freeze–Thaw Cycles for High-Performance Flexible Supercapacitors," *ACS Appl. Mater. Interfaces*, vol. 9, no. 23, pp. 20142–20149, Jun. 2017, doi: 10.1021/acsami.7b05963.
4. [4] L. Zhu, K. Uetani, M. Nogi, and H. Koga, "Polydopamine Doping and Pyrolysis of Cellulose Nanofiber Paper for Fabrication of Three-Dimensional Nanocarbon with Improved Yield and Capacitive Performances," *Nanomaterials*, vol. 11, no. 12, p. 3249, Nov. 2021, doi: 10.3390/nano11123249.
5. [5] R. R. Palem *et al.*, "Nanostructured Fe2O3@nitrogen-doped multiwalled nanotube/cellulose nanocrystal composite material electrodes for high-performance supercapacitor applications," *J. Mater. Res. Technol.*, vol. 9, no. 4, pp. 7615–7627, Jul. 2020, doi: 10.1016/j.jmrt.2020.05.058.
6. [6] N. Song, H. Tan, and Y. Zhao, "Carbon fiber-bridged polyaniline/graphene paper electrode for a highly foldable all-solid-state supercapacitor," *J. Solid State Electrochem.*, vol. 23, no. 1, pp. 9–17, Jan. 2019, doi: 10.1007/s10008-018-4109-6.
7. [7] E. G. Calvo, C. O. Ania, L. Zubizarreta, J. A. Menéndez, and A. Arenillas, "Exploring New Routes in the Synthesis of Carbon Xerogels for Their Application in Electric Double-Layer Capacitors," *Energy & Fuels*, vol. 24, no. 6, pp. 3334–3339, Jun. 2010, doi: 10.1021/ef901465j.
8. [8] K. Kraiwattanawong, H. Tamon, P. Praserthdam, "Influence of solvent species used in solvent exchange for preparation of mesoporous carbon xerogels from resorcinol and formaldehyde via subcritical drying," *Microporous Mesoporous Mater.*, vol. 138, pp. 8–16, 2011.
9. [9] M. M. L. R. C. F.L. Conçenciao, P.J.M. Carrott, "New carbon materials with high porosity in the 1–7 nm range obtained by chemical activation with phosphoric acid of resorcinol–formaldehyde aerogels," *Carbon N. Y.*, vol. 47, pp. 1874–1877, 2009.
10. [10] N. J. L. Zubizarreta, A. Arenillas, J.-P. Pirard, J.J. Pis, "Tailoring the textural properties of activated carbon xerogels by chemical activation with KOH," *Microporous Mesoporous Mater*, vol. 115, pp. 480–490, 2008.
11. [11] A. L.-S. J.A. Maciá-Agulló, B.C. Moore, D. Cazorla-Amorós, "Influence of carbon fibres crystallinities on their chemical activation by KOH and NaOH," *Microporous Mesoporous Mater.*, vol. 101, pp. 397–405, 2007.
12. [12] O. Glukhova, "Flexible Membranes for Batteries and Supercapacitor Applications," *Membranes (Basel).*, vol. 12, no. 6, p. 583, May 2022, doi: 10.3390/membranes12060583.
13. [13] H. Liu and G. Zhu, "The electrochemical capacitance of nanoporous carbons in aqueous and ionic liquids," *J. Power Sources*, vol. 171, no. 2, pp. 1054–1061, Sep. 2007, doi: 10.1016/j.jpowsour.2007.06.200.
14. [14] B. Xu *et al.*, "Room temperature molten salt as electrolyte for carbon nanotube-based electric double layer capacitors," *J. Power Sources*, vol. 158, no. 1, pp. 773–778, Jul. 2006, doi: 10.1016/j.jpowsour.2005.08.043.
15. [15] P. Liu, M. Verbrugge, and S. Soukiazian, "Influence of temperature and electrolyte on the performance of activated-carbon supercapacitors," *J. Power Sources*, vol. 156, no. 2, pp. 712–718, Jun. 2006, doi: 10.1016/j.jpowsour.2005.05.055.
16. [16] S. Maitra, R. Mitra, and T. K. Nath, "Investigation of electrochemical performance of MgNiO2 prepared by sol-gel synthesis route for aqueous-based supercapacitor application," *Curr. Appl. Phys.*, vol. 20, no. 5, pp. 628–637, May 2020, doi: 10.1016/j.cap.2020.02.013.
17. [17] Z. Wang *et al.*, "Pomelo peels-derived porous activated carbon microsheets dual-doped with nitrogen and phosphorus for high performance electrochemical capacitors," *J. Power Sources*, vol. 378, pp. 499–510, Feb. 2018, doi: 10.1016/j.jpowsour.2017.12.076.
18. [18] K. Fic, G. Lota, M. Meller, and E. Frackowiak, "Novel insight into neutral medium as electrolyte for high-voltage supercapacitors," *Energy Environ. Sci.*, vol. 5, no. 2, pp. 5842–5850, 2012, doi: 10.1039/C1EE02262H.
19. [19] M. A. Hughes, J. A. Allen, and S. W. Donne, "Optimized Electrolytic Carbon and Electrolyte Systems for Electrochemical Capacitors," *ChemElectroChem*, vol. 7, no. 1, pp. 266–282, Jan. 2020, doi: 10.1002/celc.201901202.
20. [20] S. S. Karade, S. S. Raut, H. B. Gajare, P. R. Nikam, R. Sharma, and B. R. Sankapal, "Widening potential window of flexible solid-state supercapacitor through asymmetric configured iron oxide and poly(3,4-ethylenedioxythiophene) polystyrene sulfonate coated multi-walled carbon nanotubes assembly," *J. Energy Storage*, vol. 31, p. 101622, Oct. 2020, doi: 10.1016/j.est.2020.101622.
21. [21] A. Platek-Mielczarek, J. Piwek, E. Frackowiak, and K. Fic, "Ambiguous Role of Cations in the Long-Term Performance of Electrochemical Capacitors with Aqueous Electrolytes," *ACS Appl. Mater. Interfaces*, vol. 15, no. 19, pp. 23860–23874, May 2023, doi: 10.1021/acsami.2c21926.

22. [22] N. Rey-Raap, J. Angel Menéndez, and A. Arenillas, "RF xerogels with tailored porosity over the entire nanoscale," *Microporous Mesoporous Mater.*, vol. 195, pp. 266–275, Sep. 2014, doi: 10.1016/j.micromeso.2014.04.048.
23. [23] M. K. Sahoo and G. R. Rao, "A high energy flexible symmetric supercapacitor fabricated using N-doped activated carbon derived from palm flowers," *Nanoscale Adv.*, vol. 3, no. 18, pp. 5417–5429, 2021, doi: 10.1039/D1NA00261A.
24. [24] H. Wang, J. Liu, K. Zhang, H. Peng, and G. Li, "Meso/microporous nitrogen-containing carbon nanofibers with enhanced electrochemical capacitance performances," *Synth. Met.*, vol. 203, pp. 149–155, May 2015, doi: 10.1016/j.synthmet.2015.02.013.
25. [25] B. Karamanova, A. Stoyanova, M. Shipochka, S. Veleva, and R. Stoyanova, "Effect of Alkaline-Basic Electrolytes on the Capacitance Performance of Biomass-Derived Carbonaceous Materials," *Materials (Basel).*, vol. 13, no. 13, p. 2941, Jun. 2020, doi: 10.3390/ma13132941.
26. [26] R. Yan, M. Antonietti, and M. Oschatz, "Toward the Experimental Understanding of the Energy Storage Mechanism and Ion Dynamics in Ionic Liquid Based Supercapacitors," *Adv. Energy Mater.*, vol. 8, no. 18, Jun. 2018, doi: 10.1002/aenm.201800026.
27. [27] S. Zhao, Z. Song, L. Qing, J. Zhou, and C. Qiao, "Surface Wettability Effect on Energy Density and Power Density of Supercapacitors," *J. Phys. Chem. C*, vol. 126, no. 22, pp. 9248–9256, Jun. 2022, doi: 10.1021/acs.jpcc.2c01455.
28. [28] O. N. Primachenko *et al.*, "New Generation of Compositional Aquivion®-Type Membranes with Nanodiamonds for Hydrogen Fuel Cells: Design and Performance," *Membranes (Basel).*, vol. 12, no. 9, p. 827, Aug. 2022, doi: 10.3390/membranes12090827.
29. [29] E. Y. Safronova, A. K. Osipov, and A. B. Yaroslavtsev, "Short Side Chain Aquivion Perfluorinated Sulfonated Proton-Conductive Membranes: Transport and Mechanical Properties," *Pet. Chem.*, vol. 58, no. 2, pp. 130, Feb. 2018, doi: 10.1134/S0965544118020044.
30. [30] T. S. Mathis, N. Kurra, X. Wang, D. Pinto, P. Simon, and Y. Gogotsi, "Energy Storage Data Reporting in Perspective—Guidelines for Interpreting the Performance of Electrochemical Energy Storage Systems," *Adv. Energy Mater.*, vol. 9, no. 39, Oct. 2019, doi: 10.1002/aenm.201902007.
31. [31] T. Wu, C. Hsu, Chi-Chang Hu, L. Hardwick, "Important parameters affecting the cell voltage of aqueous electrical double-layer capacitors", *J. Power Sources*, vol. 242, Nov. 2013, p. 289 - 298, https://doi.org/10.1016/j.jpowsour.2013.05.080
32. [32] O. Okhay, A. Tkach, P. Staiti, F. Lufrano, "Long term durability of solid-state supercapacitor based on reduced graphene oxide aerogel and carbon nanotubes composite electrodes", *Electrochim. Acta*, vol. 353, no.1, 136540 , Sept. 2020, https://doi.org/10.1016/j.electacta.2020.136540
33. [33] M. Boota, K.B. Hatzell, M. Alhabeb, E.C. Kumbur, Y. Gogotsi, "Graphene-containing flowable electrodes for capacitive energy storage", *Carbon*, vol. 92, pp. 142 - 149, Oct. 2015, https://doi.org/10.1016/j.carbon.2015.04.020
34. [34] Z. Wu, W. Ren, Da-Wei Wang, F. Li, B. Liu, Hui-Ming Cheng, "High-Energy MnO_2 Nanowire/ Graphene and Graphene Asymmetric Electrochemical Capacitors", *ACS Nano,* vol., 4, no.10, p. 5835, Sept. 2010, https://doi.org/10.1021/nn101754k
35. [35] H. Kim, V. Guccini, H. Lu, G. Salazar-Alvarez, G. Lindbergh, and A. Cornell, "Lithium Ion Battery Separators Based On Carboxylated Cellulose Nanofibers From Wood", *ACS Appl. Energy Mater.*, vol. 2, no. 2, pp. 1241–1250, Feb. 2019, doi: 10.1021/acsaem.8b01797.
36. [36] M. Canal-Rodríguez *et al.*, "Multiphase graphitisation of carbon xerogels and its dependence on their pore size," *Carbon N. Y.*, vol. 152, pp. 704–714, Nov. 2019, doi: 10.1016/j.carbon.2019.06.057.